

Optical properties of the Hofstadter butterfly in the Moiré superlattice

Pilkyung Moon¹ and Mikito Koshino²

¹ School of Computational Sciences, Korea Institute for Advanced Study, Seoul, 130-722, Korea

² Department of Physics, Tohoku University, Sendai, 980-8578, Japan

(Dated: November 3, 2018)

We investigate the optical absorption spectrum and the selection rule for the Hofstadter butterfly in twisted bilayer graphene under magnetic fields. We demonstrate that the absorption spectrum exhibits a self-similar recursive pattern reflecting the fractal nature of the energy spectrum. We find that the optical selection rule has a nested self-similar structure as well, and it is governed by the conservation of the total angular momentum summed over different hierarchies.

Electrons under the simultaneous influence of a periodic potential and a magnetic field exhibit a self-similar energy spectrum due to the competition between Bragg reflection and Landau quantization [1–6]. Such a fractal band structure, which is called the Hofstadter butterfly, appears when the magnetic flux Φ per a unit cell becomes as large as $\Phi_0 = h/e$. Recently, it was theoretically proposed [7–9] that the Hofstadter spectrum emerges in twisted bilayer graphene (TBG) [10–14] in moderate magnetic field, owing to a long-period Moiré pattern in the misoriented lattice structure [15]. The evidence of the fractal nature was observed in the recent magnetotransport measurements in Moiré superlattice composed of graphene and hexagonal boron nitride [16–18].

The realization of fractal energy band leads to an interest in how the optical property looks like in this unique spectrum. The magneto-optical absorption measurement has been widely used to investigate the Landau level structure of graphene systems [19–26]. For TBG, the optical spectrum at zero magnetic field was recently studied theoretically [27–31], and experimentally [27, 32], while the magneto-optical property remains to be explored. In the literature, the optical absorption of the Hofstadter butterfly was studied for a simple square lattice [33], while a detailed study is needed to specify the optical selection rule in the recursive spectrum.

The purpose of this paper is to reveal the optical absorption of the Hofstadter butterfly in TBG. TBG offers an excellent platform to investigate the fractal spectrum in optics, because the energy scale of the fractal structure can be relatively large due to the direct coupling of the two graphene bands in the low-energy region. Also, the rich variety of the spectrum sensitively depending on the rotation angle is a fascinating subject to investigate. Here we calculate the dynamical conductivity of TBG as a function of magnetic field, and demonstrate that the optical spectrum exhibits the hierarchical recursive pattern. We also find that the selection rules for optically allowed transitions exhibit a nested self-similar structure, which is governed by the conservation of the angular momentum summed over different hierarchies.

In the following, we investigate TBGs with $\theta = 2.65^\circ$

and 1.47° , where θ is the relative rotation angle between two graphene layers. The period of the Moiré superlattice is given by $L_M = a/[2\sin(\theta/2)]$ ($L_M = 5.33$ nm and 9.59 nm for $\theta = 2.65^\circ$ and 1.47° , respectively) where a is the lattice constant of graphene [13, 15, 30]. In TBG, the graphene's linear band is folded by the periodic interlayer coupling, giving the energy scale of $\varepsilon_M \sim \pi\hbar v/L_M$ with the linear band velocity v . In small rotation angles less than 2° , in particular, the energy band is strongly modified [8, 12, 14, 34–36], because ε_M becomes comparable to the magnitude of the interlayer coupling. The two rotation angles considered in this paper exhibit notably different band structures, where $\theta = 2.65^\circ$ still keeps monolayerlike dispersion near the Dirac point, while $\theta = 1.47^\circ$ exhibits an almost flat band at the Dirac point.

We model TBG with a single-orbital (carbon $2p_z$ orbital) tight-binding Hamiltonian,

$$H_{\text{TBG}} = - \sum_{\langle i,j \rangle} t(\mathbf{R}_i, \mathbf{R}_j) e^{i\phi_{ij}} |\mathbf{R}_i\rangle \langle \mathbf{R}_j| + \text{H.c.}, \quad (1)$$

where \mathbf{R}_i and $|\mathbf{R}_i\rangle$ represent the lattice point and the atomic state at site i , respectively, $t(\mathbf{R}_i - \mathbf{R}_j)$ is the transfer integral between site i and site j . The phase factor $\phi_{ij} = -(e/\hbar) \int_j^i \mathbf{A}(\mathbf{r}) \cdot d\mathbf{r}$ is a Peierls phase where $\mathbf{A}(\mathbf{r}) = (0, Bx, 0)$ is the vector potential giving a uniform magnetic field B perpendicular to the layers. For $t(\mathbf{R})$, we adopt an approximation [8, 12, 30, 37],

$$-t(\mathbf{d}) = V_{pp\pi}(d) \left[1 - \left(\frac{\mathbf{d} \cdot \mathbf{e}_z}{d} \right)^2 \right] + V_{pp\sigma}(d) \left(\frac{\mathbf{d} \cdot \mathbf{e}_z}{d} \right)^2, \\ V_{pp\pi}(d) = V_{pp\pi}^0 e^{-\frac{d-a_0}{r_0}}, \quad V_{pp\sigma}(d) = V_{pp\sigma}^0 e^{-\frac{d-d_0}{r_0}}, \quad (2)$$

where $V_{pp\pi}^0 \approx -2.7$ eV is the transfer integral between the nearest-neighbor atoms of monolayer graphene, and $V_{pp\sigma}^0 \approx 0.48$ eV is that between vertically located atoms on the neighboring layers. r_0 is the decay length of the transfer integral, and is chosen as 0.045 nm so that the next nearest intralayer coupling becomes $0.1V_{pp\pi}^0$ [21]. $a_0 \approx 0.142$ nm is the distance between the nearest carbon atoms in graphene, and $d_0 \approx 0.335$ nm is the interlayer spacing.

The other three orbitals of carbon ($2s$ orbital and two $2p$ orbitals) are safely ignored, since they form sp_2 hy-

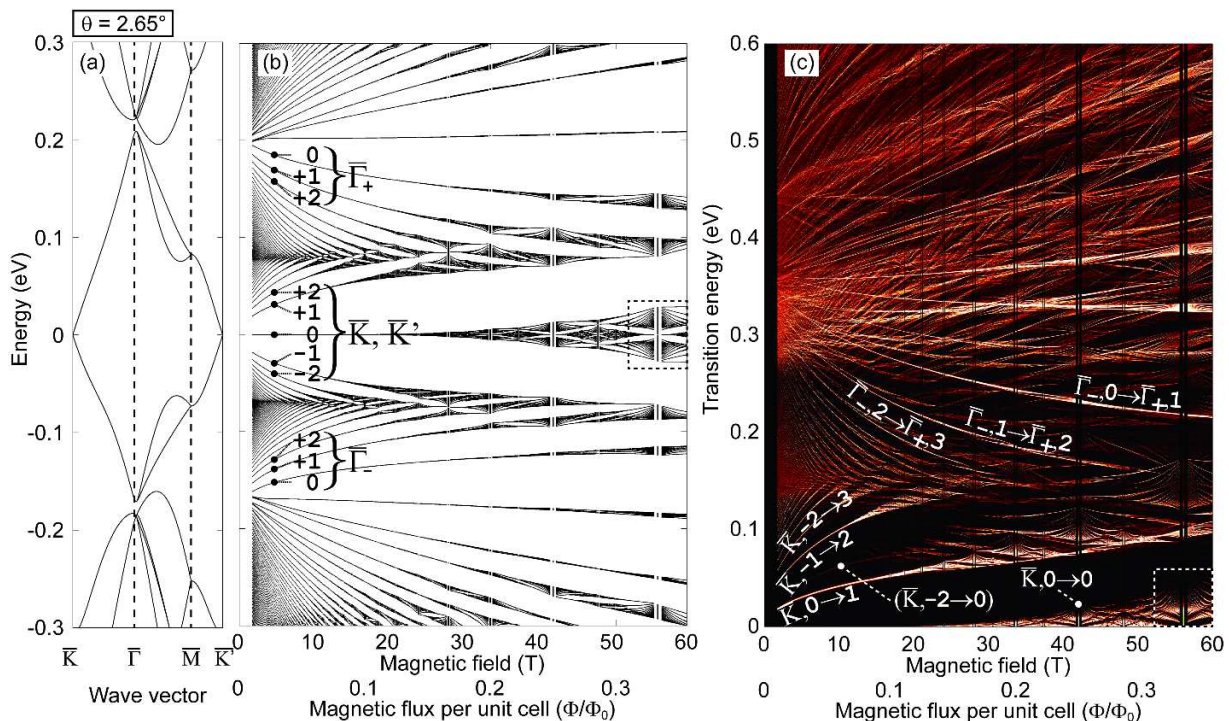


FIG. 1: (a) Band structure at $B = 0$ T and (b) energy spectrum as a function of B , calculated for TBG with $\theta = 2.65^\circ$. (c) Intensity map of the optical conductivity for right circularly polarized light ($\text{Re } \sigma_+$) of the same TBG.

bridized orbitals of which energies are far from Dirac point. The single-orbital tight-binding method has been widely used to investigate electronic properties of carbon-based materials (e.g., graphite, carbon nanotube, and graphene) [38–41], and the approximate values of the parameters are well established [38].

For the basis to construct the Hamiltonian matrix, we only take the wavefunctions of low-lying Landau levels of monolayer graphene in $|\varepsilon| \lesssim 1.5$ eV, and compose the Hamiltonian matrix by writing H_{TBG} in terms of the reduced basis [8]. The dynamical conductivities for right (σ_+) and left (σ_-) circularly polarized light can be obtained by [42, 43]

$$\sigma_{\pm}(\omega) = \frac{e^2 \hbar}{iS} \sum_{\alpha, \beta} \frac{f(\varepsilon_{\alpha}) - f(\varepsilon_{\beta})}{\varepsilon_{\alpha} - \varepsilon_{\beta}} \frac{|\langle \alpha | v_{\pm} | \beta \rangle|^2}{\varepsilon_{\alpha} - \varepsilon_{\beta} + \hbar\omega + i\eta} \quad (3)$$

where S is the area of the system, $f(\varepsilon)$ is the Fermi distribution function, ε_{α} (ε_{β}) and $|\alpha\rangle$ ($|\beta\rangle$) represent the eigenenergy and the eigenstate of the system, $v_{\pm} = (v_x \pm iv_y)/\sqrt{2}$, $v_x = -(i/\hbar)[x, H]$ is the velocity operator, and η is a phenomenological broadening which is taken as $\eta = 0.05$ meV for $\theta = 2.65^\circ$ and 0.025 meV for 1.47° . The optical absorption intensity of incident light perpendicular to a two-dimensional system, at photon energies $\hbar\omega$, is approximately given by $(4\pi/c)\text{Re } \sigma_{\pm}(\omega)$. We fix the temperature to 0 and assume the Fermi energy at the charge neutrality point.

Figure 1(a) shows the band structure of TBG with $\theta = 2.65^\circ$ at zero magnetic field. \bar{K} , \bar{K}' , \bar{M} , and $\bar{\Gamma}$ represent the high-symmetry points of the reduced Brillouin zone of TBG. The lowest conduction and valence bands, lying in the energy range from -0.2 eV to 0.2 eV, are characterized by the monolayerlike linear dispersion near \bar{K} and \bar{K}' , saddle point at \bar{M} , and a holelike (electron-like) pocket in the conduction (valence) band at $\bar{\Gamma}$ [8, 30].

In Fig. 1(b), we plot the energy spectrum against the magnetic field B for the same TBG. In weak magnetic field, the lowest conduction band is composed of monolayerlike Landau levels at \bar{K} and \bar{K}' which behave in proportion to \sqrt{B} , and also the holelike Landau levels at $\bar{\Gamma}$ which move downward in increasing B [8]. We label the Landau levels at \bar{K}, \bar{K}' by (\bar{K}, n) and (\bar{K}', n) with $n = 0, \pm 1, \pm 2, \dots$, and those associated with $\bar{\Gamma}$ by $(\bar{\Gamma}_+, n)$ and $(\bar{\Gamma}_-, n)$ with $n = 0, 1, 2, \dots$, for the positive and the negative energy parts, respectively. The labeling of the Landau levels is indicated in Fig. 1(b).

Figure 1(c) shows a density plot of the optical absorption intensity for circularly polarized light ($\text{Re } \sigma_+$) on the space of the transition energy $\hbar\omega$ and the magnetic field B , calculated for TBG with $\theta = 2.65^\circ$. The spectrum in the weak field regime ($\Phi/\Phi_0 < 0.1$) consists of sharp peaks associated with the transitions between discrete Landau levels. Below the transition energy of $\hbar\omega \approx 0.15$ eV, which is the energy span between the van Hove singularities in Fig. 1(a), we observe the monolayer-

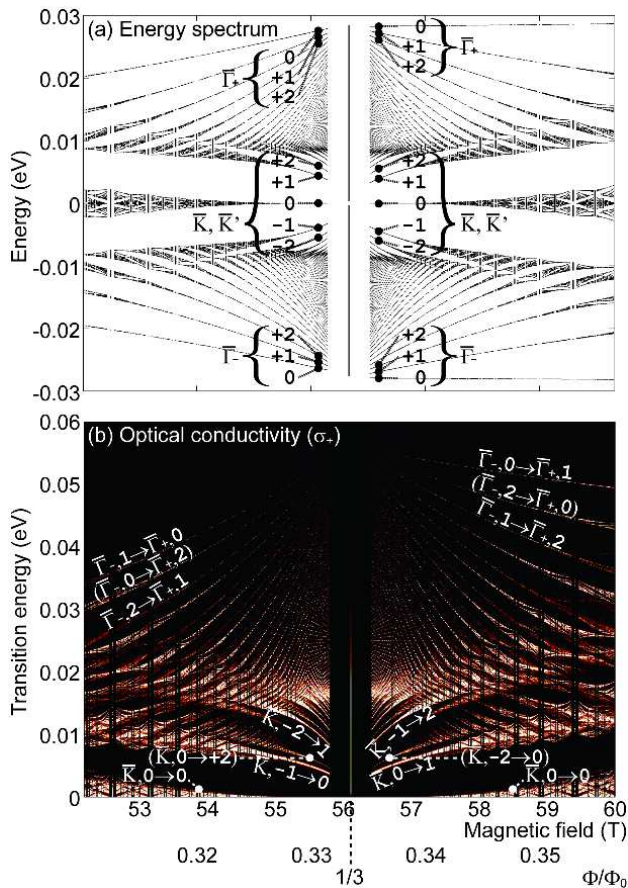


FIG. 2: (a) Energy spectrum and (b) optical conductivity for right circularly polarized light ($\text{Re } \sigma_+$) of TBG with $\theta = 2.65^\circ$, near the $n = 0$ Landau level around $\Phi/\Phi_0 = 1/3$ [the regions marked by dashed boxes in Figs. 1(b) and (c)].

erlike absorption peaks corresponding to the transitions from $(\bar{K}, -n)$ to $(\bar{K}, n+1)$. Above 0.15 eV, we can see the series of spectral lines which go down with increasing B , and they are associated with the transitions from $(\bar{\Gamma}_-, n)$ to $(\bar{\Gamma}_+, n+1)$. The transitions between the different families of Landau levels, such as $\bar{K} \rightarrow \bar{\Gamma}_+$, are negligibly small.

The selection rule for the optically allowed transition is expressed as $|n| \rightarrow |n| + 1$ in either transition series. This is because the relative angular momentum of a state in the Landau level n_2 to one in n_1 with the same center coordinate is $(|n_2| - |n_1|)\hbar$ regardless of the electronlike or holelike level, and a right circularly polarized photon carries an angular momentum of $+\hbar$. For the left circularly polarized light (σ_-), the photon's angular momentum becomes $-\hbar$ and the selection rule changes to $|n| \rightarrow |n| - 1$. In TBG, the absorption peak positions generally differ between σ_+ and σ_- (not shown) because of the electron-hole asymmetry in the energy spectrum [30, 34]. The system should exhibit a significant circular dichroism when the frequency hits a peak of σ_+ or σ_- .

Besides the major peaks described by the above selection rule, we also observe additional, minor peaks corresponding to the transition $|n| \rightarrow |n| + 3m + 1$ (m : integer). This is a direct consequence of the trigonal warping of zero-field band structure which hybridizes $|n|$ and $|n| + 3$ [24, 44]. The optical spectrum above $\hbar\omega \sim 0.3$ eV is complicated because it includes the absorption peaks associated with the Landau levels in the higher energy band.

In increasing magnetic field, as we can see from Fig. 1(b), the spectrum evolves into Hofstadter butterfly, where each Landau level splits into sub-generation levels with a smaller energy scale. The optical spectrum in Fig. 1(c) also evolves into a fractal structure in this regime, reflecting the hierarchy of the recursive energy structures. The spectrum is characterized by Φ/Φ_0 , i.e., the number of flux quanta penetrating the Moiré unit cell, where each Landau level forms $2p$ subbands when Φ/Φ_0 is a rational number p/q (p and q are coprime integers). Here the factor 2 in $2p$ comes from the number of layers.

Figure 2 shows the energy and optical spectra near the $n = 0$ Landau level around $\Phi/\Phi_0 = 1/3$, corresponding to the regions enclosed by the dashed boxes in Figs. 1(b) and (c). At $\Phi/\Phi_0 = 1/3$, the $n = 0$ Landau level becomes a pair of energy bands touching at the zero energy, and the energy dispersion in the magnetic Brillouin zone is shown to have a similar structure to the lowest energy band at $B = 0$ T. When the flux is shifted from $1/3$, the band splits into the second-generation Landau levels, which can be labeled by (\bar{K}, n') and $(\bar{\Gamma}_\pm, n')$ as shown in Fig. 2(a), similarly to the first-generation Landau levels. Correspondingly, the optical spectrum in $\Phi/\Phi_0 > 1/3$ in Fig. 2(b) resembles that for the first-generation in $\Phi/\Phi_0 > 0$, and the selection rule becomes $|n'| \rightarrow |n'| + 1$. We also see the additional excitations $|n'| \rightarrow |n'| + 1 + 3m$ due to the trigonal warping.

It should be noted that these transitions occur inside the same parent Landau level $n = 0$, which were originally forbidden in the weak magnetic field $\Phi/\Phi_0 < 0.1$. They come to be allowed in the butterfly regime, because the second-generation Landau levels have the additional angular momentum depending on n' , and can absorb the photon's angular momentum. In $\Phi/\Phi_0 < 1/3$, the selection rule becomes $|n'| \rightarrow |n'| - 1$, since the residual magnetic field from $\Phi/\Phi_0 = 1/3$ is negative, and the angular momenta for the second-generation Landau levels reverse the sign. The same structure can be seen also at $\Phi/\Phi_0 = 1/q$ for every integer q .

We also have the transitions between the sub-Landau levels belonging to different parent Landau levels. The global address for an energy level near $\Phi/\Phi_0 = 1/q$ is written like $(n; \bar{K}, n')$ or $(n; \bar{\Gamma}_\pm, n')$, etc., where n and n' are the Landau level indices for the first generation and the second generation, respectively. The transition occurs only inside the same valley \bar{K} , \bar{K}' and $\bar{\Gamma}$ ($\bar{\Gamma}_\pm \rightarrow \bar{\Gamma}_\pm$ and $\bar{\Gamma}_\pm \rightarrow \bar{\Gamma}_\mp$ are both allowed). In $\Phi/\Phi_0 \geq 1/q$,

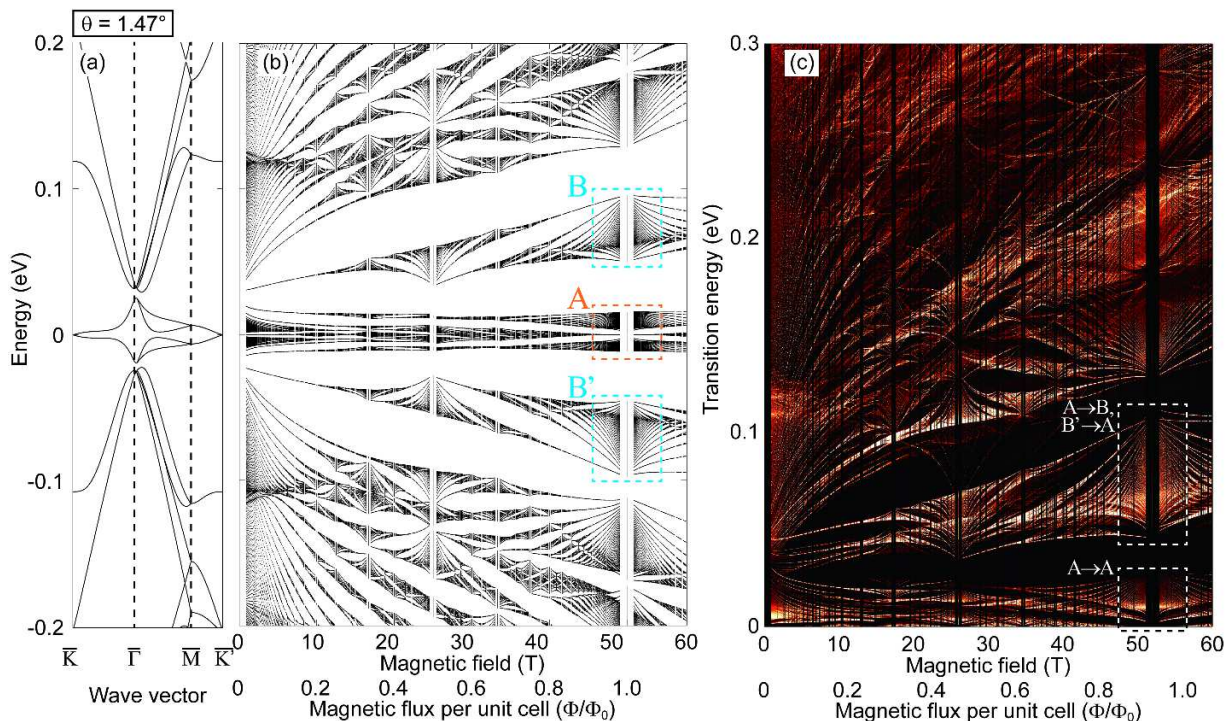


FIG. 3: (a) Band structure at $B = 0$ T and (b) energy spectrum as a function of B , calculated for TBG with $\theta = 1.47^\circ$. (c) Intensity map of the optical conductivity ($\text{Re } \sigma_+$) of the same TBG.

the selection rule is found to be $|n_i| + |n'_i| + 1 = |n_f| + |n'_f|$ (in modulo 3), where i and f are for the initial and final states, respectively, indicating that the total angular momentum is written as the sum over the first and the second generations. In $\Phi/\Phi_0 \leq 1/q$, the selection rule changes to $|n_i| - |n'_i| + 1 = |n_f| - |n'_f|$ (in modulo 3), because the sign of the angular momentum in the second-generation level becomes opposite.

The condition to observe the sub-generation Landau levels can be estimated by comparing the width of Moiré-modulated Landau level (w) and the disorder broadening (Γ). For zero-th Landau level, for example, the order of w is estimated as $w \sim V_{pp\sigma}^0 e^{-\pi/(3\sqrt{3}\Phi)}$, when the inter Landau level mixing is not very strong. When Φ exceeds 0.1, w rapidly grows from an exponentially small value to a significant magnitude. In the long-range disorder potential, Γ is shown to be proportional to \sqrt{B} [45], so that the condition $w > \Gamma$ is more easily achieved in the higher magnetic field. In short-range scatterers such as vacancies, on the other hand, the low-lying Landau levels are strongly broadened by the impurity levels at zero energy [46], and it may mask the butterfly structure near the zero-th Landau level.

Figure 3 shows the energy spectrum and the optical absorption spectrum of TBG with a smaller rotation angle $\theta = 1.47^\circ$. The lowest energy band shrinks drastically near the Dirac point in this case [12], and the monolay-

erlike absorption peaks are almost invisible. Instead, the fractal spectrum is clearly seen in smaller magnetic field than in $\theta = 2.65^\circ$, due to the larger Moiré superlattice period. At the magnetic flux $\Phi/\Phi_0 = 1$, the regions A, B and B' [enclosed by dashed boxes in Fig. 3(b)] belong to the original monolayer's Landau levels of $n = 0, 1$ and -1 , respectively. In the optical absorption spectrum, Fig. 3(c), the low-energy peaks are attributed to the transitions between these blocks, and the optical transition between second-generation Landau levels is governed by the selection rule discussed above.

We have theoretically investigated the optical absorption spectra of Hofstadter butterfly in TBG under magnetic field. In weak magnetic field, the absorption spectrum consists of sharp peaks associated with the transitions between discrete Landau levels. In increasing magnetic field, the spectrum gradually evolves into a fractal structure, reflecting the hierarchy of the recursive energy spectrum. We have shown that the optical selection rule exhibits a nested self-similar structure, which is governed by the conservation of the angular momentum summed over different hierarchies.

Computational resources have been provided by CAC of KIAS (P.M.). This project has been funded by JSPS Grant-in-Aid for Scientific Research No. 24740193 and No. 25107005 (M.K.).

-
- [1] J. Zak, *Physical Review* **134**, 1602 (1964).
- [2] D. Langbein, *Phys. Rev.* **180**, 633 (1969).
- [3] D. Hofstadter, *Phys. Rev. B* **14**, 2239 (1976).
- [4] T. Schlösser, K. Ensslin, J. Kotthaus, and M. Holland, *Europhys. Lett.* **33**, 683 (1996).
- [5] C. Albrecht, J. Smet, K. von Klitzing, D. Weiss, V. Umansky, and H. Schweizer, *Phys. Rev. Lett.* **86**, 147 (2001).
- [6] M. Geisler, J. Smet, V. Umansky, K. von Klitzing, B. Naundorf, R. Ketzmerick, and H. Schweizer, *Phys. Rev. Lett.* **92**, 256801 (2004).
- [7] R. Bistritzer and A. MacDonald, *Phys. Rev. B* **84**, 35440 (2011).
- [8] P. Moon and M. Koshino, *Phys. Rev. B* **85**, 195458 (2012).
- [9] Z. Wang, F. Liu, and M. Chou, *Nano lett.* **12**, 3833 (2012).
- [10] J. Lopes dos Santos, N. Peres, and A. Castro Neto, *Phys. Rev. Lett.* **99**, 256802 (2007).
- [11] J. Hass, F. Varchon, J. Millan-Otoya, M. Sprinkle, N. Sharma, W. de Heer, C. Berger, P. First, L. Magaud, and E. Conrad, *Phys. Rev. Lett.* **100**, 125504 (2008).
- [12] G. Trambly de Laissardière, D. Mayou, and L. Magaud, *Nano lett.* **10**, 804 (2010).
- [13] S. Shallcross, S. Sharma, E. Kandelaki, and O. Pankratov, *Phys. Rev. B* **81**, 165105 (2010).
- [14] E. Morell, J. Correa, P. Vargas, M. Pacheco, and Z. Barticevic, *Phys. Rev. B* **82**, 121407 (2010).
- [15] K. Hermann, *J. Phys.: Condens. Matter* **24**, 314210 (2012).
- [16] C. Dean, L. Wang, P. Maher, C. Forsythe, F. Ghahari, Y. Gao, J. Katoch, M. Ishigami, P. Moon, M. Koshino, et al., *Nature* **497**, 598 (2013).
- [17] L. Ponomarenko, R. Gorbachev, G. Yu, D. Elias, R. Jalil, A. Patel, A. Mishchenko, A. Mayorov, C. Woods, J. Wallbank, et al., *Nature* **497**, 594 (2013).
- [18] B. Hunt, J. Sanchez-Yamagishi, A. Young, K. Watanabe, T. Taniguchi, P. Moon, M. Koshino, P. Jarillo-Herrero, and R. Ashoori, *Science* (2013).
- [19] M. Sadowski, G. Martinez, M. Potemski, C. Berger, and W. de Heer, *Phys. Rev. Lett.* **97**, 266405 (2006).
- [20] Z. Jiang, E. Henriksen, L. Tung, Y.-J. Wang, M. Schwartz, M. Han, P. Kim, and H. Stormer, *Phys. Rev. Lett.* **98**, 197403 (2007).
- [21] R. Deacon, K.-C. Chuang, R. Nicholas, K. Novoselov, and A. Geim, *Phys. Rev. B* **76**, 081406 (2007).
- [22] P. Plochocka, C. Faugeras, M. Orlita, M. L. Sadowski, G. Martinez, M. Potemski, M. O. Goerbig, J.-N. Fuchs, C. Berger, and W. A. De Heer, *Phys. Rev. Lett.* **100**, 087401 (2008).
- [23] V. Gusynin and S. Sharapov, *Phys. Rev. B* **73**, 245411 (2006).
- [24] D. S. L. Abergel and V. I. Fal'ko, *Phys. Rev. B* **75**, 155430 (2007).
- [25] M. Koshino and T. Ando, *Phys. Rev. B* **77**, 115313 (2008).
- [26] I. Crassee, J. Levallois, A. Walter, M. Ostler, A. Bostwick, E. Rotenberg, T. Seyller, D. Van Der Marel, and A. Kuzmenko, *Nature Phys.* **7**, 48 (2010).
- [27] Y. Wang, Z. Ni, L. Liu, Y. Liu, C. Cong, T. Yu, X. Wang, D. Shen, and Z. Shen, *ACS nano* **4**, 4074 (2010).
- [28] Z. Chen and X. Wang, *Phys. Rev. B* **83**, 081405 (2011).
- [29] C. J. Tabert and E. J. Nicol, *Phys. Rev. B* **87**, 121402 (2013).
- [30] P. Moon and M. Koshino, *Phys. Rev. B* **87**, 205404 (2013).
- [31] T. Stauber, P. San-Jose, and L. Brey, arXiv:1307.4606 (2013).
- [32] T. Ohta, J. Robinson, P. Feibelman, A. Bostwick, E. Rotenberg, and T. Beechem, *Phys. Rev. Lett.* **109**, 186807 (2012).
- [33] P. Vogl and C. Strahberger, *Phys. Status Solidi (b)* **234**, 472 (2002).
- [34] A. Luican, G. Li, A. Reina, J. Kong, R. Nair, K. Novoselov, A. Geim, and E. Andrei, *Phys. Rev. Lett.* **106**, 126802 (2011).
- [35] R. Bistritzer and A. MacDonald, *Proc. Natl. Acad. Sci.* **108**, 12233 (2011).
- [36] A. MacDonald and R. Bistritzer, *Nature* **474**, 453 (2011).
- [37] J. Slater and G. Koster, *Phys. Rev.* **94**, 1498 (1954).
- [38] M. S. Dresselhaus and G. Dresselhaus, *Adv. Phys.* **51**, 1 (2002).
- [39] T. Ando, *J. Phys. Soc. Jpn.* **74**, 777 (2005).
- [40] A. Neto, F. Guinea, N. Peres, K. Novoselov, and A. Geim, *Rev. Mod. Phys.* **81**, 109 (2009).
- [41] N. Peres, *Rev. Mod. Phys.* **82**, 2673 (2010).
- [42] M. Inoue, *J. Phys. Soc. Jpn.* **17**, 808 (1962).
- [43] W. Toy, M. Dresselhaus, and G. Dresselhaus, *Phys. Rev. B* **15**, 4077 (1977).
- [44] T. Morimoto, M. Koshino, and H. Aoki, *Phys. Rev. B* **86**, 155426 (2012).
- [45] N. H. Shon and T. Ando, *J. Phys. Soc. Jpn.* **67**, 2421 (1998).
- [46] N. Peres, F. Guinea, and A. Neto, *Phys. Rev. B* **73**, 125411 (2006).